

# Polarization of cosmic microwave background scattered by moving flat protoobjects

N.N. Shakhvorostova<sup>1</sup>, S.I. Grachev<sup>2</sup>, V.K. Dubrovich<sup>3</sup>

October 29, 2018

<sup>1</sup>Astro-Space Center, Lebedev's Physical Institute, Moscow, Russia

<sup>2</sup>Saint-Petersburg State University, Sobolev Astronomical Institute, Saint-Petersburg, Russia

<sup>3</sup>Special Astrophysical Observatory, Saint-Petersburg Department, Saint-Petersburg, Russia

The work is devoted to the investigations of possible observational manifestations of protoobjects related to “dark ages” epoch ( $10 < z < 1000$ ), before formation of self-luminous galaxies and stars. These objects can distort the cosmic microwave background. Formation of these objects is described in the “pancake theory” and in the model of “hierarchic clustering”. According to these theories we may consider these protoobjects as flat layers.

We consider both Thomson (with Rayleigh phase matrix) and resonance (for complete frequency redistribution) scattering of cosmic microwave background radiation by moving flat layer. The appearing anisotropy and polarization of cosmic microwave radiation are calculated for a wide range of a layer optical thicknesses (from optically thin layer to optically thick one). Analytical solutions are also obtained for the case of an optically thin layer and are compared with the numerical ones.

## 1 Introduction

We consider a special period in the Universe evolution extending from recombination epoch ( $z = 1000$ ) till the time of self-emitting stars and galaxies formation ( $z = 10$ ). This period is called “dark ages” and the question about possible observational manifestations of dark objects from that period is actual. One of the most effective ways to solve this problem is to try to observe the cosmic microwave background (CMB) distortions caused by these objects, as it was firstly reported in [1]. The character of such distortions is defined by the physical properties of “dark ages” objects, which are naturally the protoclusters of galaxies [2].

Now two basic theories of galaxy clusters formation are being discussed. The first one, so called “pancake theory”, was suggested by Ya.B. Zeldovich (see [3] for example) and further developed in some papers (see [4], [5]). According to this theory, the substance is collapsing into flat formations — “pancakes” (protoclusters). Initial shock waves forming in this process can be modelled as flat layers. According to the second theory, “the model of hierarchic clustering” [6], small structures are merging into larger ones (“the boxes”). These structures contain a large number of small dense objects merging to form present galaxies and diffuse gas substance. The difference between these two galaxy clusters formation models consists only in the value of mass ratio of dense objects and diffuse substance. In the first theory gas “pancakes” contain the most part of the total mass, and in the second one the most but not the whole mass is contained in dense objects. Therefore, the gas mass is not equal to zero and its spatial distribution as flat “pancakes” takes place in both theories and we may consider them as flat layers.

Possible distortions of CMB appear due to the fact that these flat layers can move relatively CMB with peculiar velocities (see [7] for example). Due to the Doppler effect caused by this motion the CMB becomes anisotropic in the reference frame of the layer. This anisotropy, which is axially symmetric with respect to the direction of the motion, leads to polarization and intensity changes of scattered radiation. These distortions belong to the “secondary CMB distortions”. Their differences from ones forming at the hydrogen recombination time ( $z = 1000$ ) consist in other angular scales and possibly in a more complicated spectrum. In particular, “secondary fluctuations” can appear not only due to the scattering on electrons, but on primary molecules as well [8], [9], [10].

Peculiar velocities of substance large scale fluctuations for a wide range of cosmological models can be estimated by the formula [11], [12]:

$$v_p = 600 (1 + z)^{-1/2} \text{ km/s}, \quad (1)$$

where the numerical coefficient is obtained as a result of a large number of velocity estimations of nearby clusters of galaxies. The velocity dependence on  $z$  is defined by the general law of the massive body motion in the expanding Universe. The calculation of the optical depth is different for scattering on free electrons (Thomson scattering) and for resonance scattering on atoms, ions or molecules. Thomson optical depth does not depend on the wavelength and is defined by the size of density fluctuation and electron density. The last quantity sufficiently depends on the redshift: after the hydrogen recombination at  $z = 1300$  the fractional electrons density falls from the unity to the value about 0.01% at  $z = 100$ . But after that time the number of free electrons rises due to the secondary ionization the details of which are being investigated by several authors and may sufficiently differ in various models (see [13] for example). Observational restrictions based on the power spectrum of primary CMB fluctuations give for the average optical thickness of such objects  $\tau_0 < 0.1$ . However, it can achieve unity for particular objects.

Existence of free electrons and protons leads automatically to the appearance of bremsstrahlung not related with the peculiar velocity. The role of such emission in the secondary ionization epoch was investigated in [14] where it was pointed out that there is a quite wide range of fluctuation parameters for which the role of this process is very small.

As concerned a resonance scattering in molecular lines there is a strong dependency of observed effect on the frequency. The estimation of the optical thickness of the layer (averaged over the line)  $\tau_0$  in this case is much more complicated problem since the density of different molecules strongly depends on physical processes in a given epoch [9]. In principle, the estimation of second type shocks efficiency (excitation and disactivation by collisions with electrons and atoms) is necessary here. However, we may neglect such processes for the considered epoch because of a very low absolute concentration of colliding particles (numerical estimates are made in [9]). Thus, in a first approximation we may consider only the Doppler mechanism of CMB distortions formation. CMB interaction with molecules having high dipole moments will be most effective. From this point of view the main attention was paid to the molecules  $HD^+$ ,  $HeH^+$ ,  $LiH$  and some other ones [1], [15]. A large number of  $HeH^+$  molecules can be formed in the shock wave at the stage of nonlinear collapse of primary “pancakes”. This way to observe the large scale distribution of substance at  $z \sim 10$  appears to be possible. The role of other molecules is many times less (see [10] for example). The lines of rotational and vibrational transitions of such molecules at  $z \sim 200$  can be situated in a millimeter range. The discovery of two lines of rotational-vibrational array should allow to define the type of molecule and  $z$ .

The effects of CMB scattering on free electrons in the hot intergalactic gas of rich clusters of galaxies were considered in the papers by Zeldovich and Sunyaev [16], [17], [18], where the analytical estimates of CMB polarization caused both by the gas motion and by the intrinsic anisotropy of CMB were obtained. Those papers were principally based on a single scattering assumption which, however, leads to polarization which is proportional only to  $(v/c)^2$ . Analytical estimate of  $O(v/c)$  effects with account of double scattering for moving spherical objects was made in [16].

The primary goal of our work is the numerical calculation of CMB distortion effects depending on the layer parameters with no restriction concerning to the number of scatterings taken into account. We consider both Thomson (with Rayleigh phase matrix) and resonance (for complete frequency redistribution) scattering of cosmic microwave background by moving flat layer. The appearing anisotropy and polarization of cosmic microwave radiation are calculated for a wide range of a layer optical thicknesses (from optically thin layer to optically thick one). Analytical solutions are also obtained for the case of an optically thin layer and are compared with the numerical solutions. Since the electron number density after the recombination epoch becomes too small, this mechanism will be more effective at the beginning of nonlinear stage of protoobjects evolution at the “secondary ionization” epoch ( $10 < z < 50$ ) (see [11] for example). The molecular scattering can play sufficient role at  $z < 150$ .

The predicted effects can be observed in a wide range of angular sizes which depend on cosmological model parameters and may vary from dozens of angular seconds to dozens of angular minutes.

## 2 Rayleigh scattering

Let us consider plane-parallel horizontally homogeneous layer moving as a whole with a velocity  $\mathbf{v}$  (with regard to CMB) at the direction of an outer normal  $\mathbf{n}$  to the layer. According to eq. (1) peculiar velocities of such objects

are about 150 km/s. Thus, we may assume  $v/c \ll 1$  and disregard the terms of the order of  $(v/c)^2$  in further calculations. The layer is illuminated by CMB with the intensity (in its own reference frame) described by Planck function with the temperature  $T = 2.7K$ . Having transformed to the layer reference frame the CMB intensity is given by

$$I(\mu, \nu) = \frac{2h\nu^3}{c^2} \frac{1}{e^{\gamma(1+\mu\beta)h\nu/kT} - 1}, \quad (2)$$

where  $\nu$  is the radiation frequency,  $\mu$  is the cosine of the angle between the velocity and radiation propagation directions in the layer reference frame,  $\beta = v/c$ ,  $\gamma = 1/\sqrt{1-\beta^2}$ .

Since we have azimuthal-symmetric picture, the field of radiation is completely described by two-component Stokes vector  $\mathbf{i} = (I, Q)^T$ , where “T” means matrix transposition,  $I = I(r, \mu, \nu)$ ,  $Q = Q(r, \mu, \nu)$ ,  $r$  is the distance from one of the layer borders.

In the case of Rayleigh scattering we will use the optical depth  $\tau$  as the geometric variable instead of  $r$ :  $d\tau = -n_e\sigma dr$  and denote the layer optical thickness as  $\tau_0$ . Here  $n_e$  is the electron density,  $\sigma$  is the Thomson cross-section. Since the picture is independent of frequency, the Stokes vector can be written as  $\mathbf{i}(\tau, \mu) = (I(\tau, \mu), Q(\tau, \mu))^T$ . This vector is the solution of radiative transfer equation ([19], [20])

$$\mu \frac{\partial \mathbf{i}(\tau, \mu)}{\partial \tau} = \mathbf{i}(\tau, \mu) - (1/2) \int_{-1}^1 \hat{P}(\mu, \mu') \mathbf{i}(\tau, \mu') d\mu' - \mathbf{s}^*(\tau, \mu) \equiv \mathbf{i}(\tau, \mu) - \mathbf{s}(\tau, \mu) \quad (3)$$

with the boundary conditions

$$\mathbf{i}(0, \mu) = \mathbf{i}_1(\mu), \quad \mu < 0; \quad \mathbf{i}(\tau_0, \mu) = \mathbf{i}_2(\mu), \quad \mu > 0, \quad (4)$$

where  $\mathbf{i}_1(\mu)$  and  $\mathbf{i}_2(\mu)$  are the Stokes vectors of radiation illuminating the layer from outside at the boundaries  $\tau = 0$  and  $\tau = \tau_0$ , respectively. Here  $\mathbf{s}^*$  characterizes primary sources distribution in the layer and the phase matrix  $\hat{P}(\mu, \mu')$  is, in general, the superposition of the Rayleigh phase matrix  $\hat{P}_R$  and the phase matrix of isotropic scattering  $\hat{P}_I$ :  $\hat{P} = (1 - W)\hat{P}_I + W\hat{P}_R$ . Here  $W$  is the depolarization parameter which is usually in the range  $[0, 1]$ . For the phase matrix the following factorization is obtained (see [20]):  $\hat{P}(\mu, \mu') = \hat{A}(\mu)\hat{A}^T(\mu')$ , where the matrix

$$\hat{A}(\mu) = \begin{pmatrix} 1 & b(1 - 3\mu^2) \\ 0 & 3b(1 - \mu^2) \end{pmatrix}. \quad (5)$$

Here and below  $b = \sqrt{W/8}$ . In the case of Rayleigh scattering considered here the depolarization parameter  $W$  is equal to 1.

Taking into account a single scattering of an outer radiation and using the phase matrix factorization, we reduce the problem to the solution of eq. (3) with the free term

$$\mathbf{s}^*(\tau, \mu) = (1/2)\hat{A}(\mu) \int_0^1 \hat{A}^T(\mu') \left[ e^{-(\tau_0-\tau)/\mu'} \mathbf{i}_2(\mu') + e^{-\tau/\mu'} \mathbf{i}_1(-\mu') \right] d\mu' \quad (6)$$

and zero boundary conditions

$$\mathbf{i}(0, \mu) = 0, \quad \mu < 0; \quad \mathbf{i}(\tau_0, \mu) = 0, \quad \mu > 0. \quad (7)$$

For  $\mathbf{i}_1(\mu)$  and  $\mathbf{i}_2(\mu)$  we use the expansion of background radiation in the layer reference frame (2) with the accuracy of the order of  $O(v/c)$ :

$$\mathbf{i}_1(\mu) = \mathbf{i}_2(\mu) \sim B(\nu, T) [1 - (v/c)a_\nu\mu] \mathbf{e}_1, \quad (8)$$

where  $a_\nu = xe^x/(e^x - 1)$ ,  $x = h\nu/kT$ ,  $\mathbf{e}_1 = (1, 0)^T$ .

According to eq. (8) we divide the both sides of the main equation (3) by the depth independent factor  $B(\nu, T)$  so that below the Stokes vector  $\mathbf{i}(\tau, \mu)$  and the vector source function  $\mathbf{s}(\tau, \mu)$  are dimensionless (measured in the units of  $B(\nu, T)$ ).

The factorization of the phase matrix  $\hat{P}(\mu, \mu')$  leads evidently to factorization of the source term in the righthandside of eq. (3):  $\mathbf{s}(\tau, \mu) = \hat{A}(\mu)\mathbf{s}(\tau)$ . Then we use the procedure described in [20] to reduce the problem to the solution of the linear integral equation for a vector source function  $\mathbf{s}(\tau)$  depending only on the optical depth.

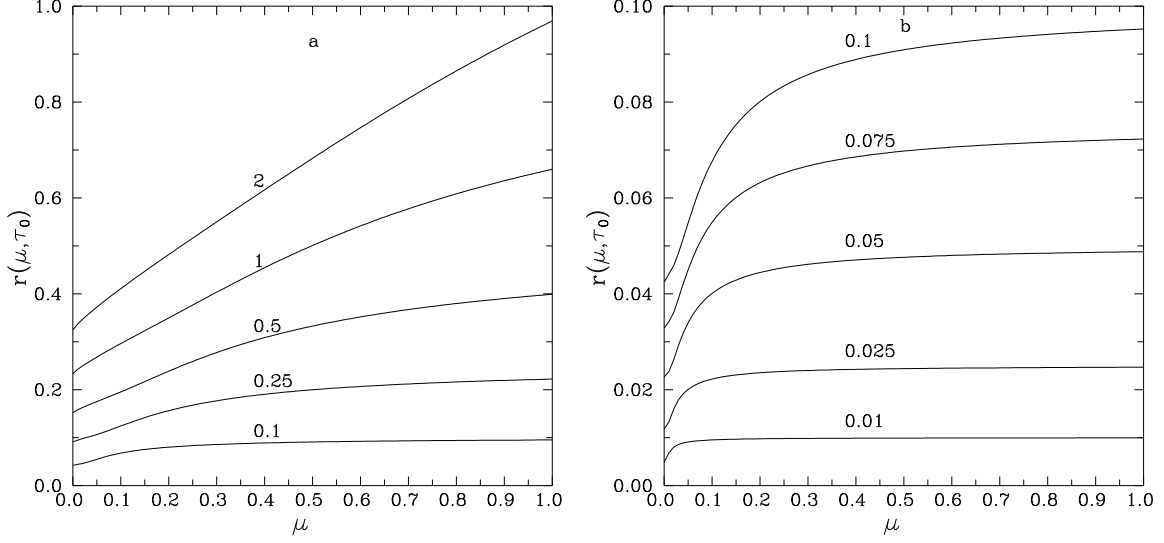


Figure 1: Profiles of intensity change for Rayleigh scattering for different values of  $\tau_0$  marked near the curves.

Finally we obtain the following expression for the Stokes vector of radiation emerging through the boundary  $\tau = 0$  (for the observer reference frame):

$$\mathbf{i}(0, \mu) = \mathbf{e}_1 + (v/c)a_\nu\mu \left(1 - e^{-\tau_0/\mu}\right) \mathbf{e}_1 + (v/c)a_\nu\hat{A}(\mu) \int_0^{\tau_0} e^{-\tau/\mu} \mathbf{s}(\tau) d\tau/\mu, \quad \mu > 0, \quad (9)$$

where  $\mathbf{s}(\tau) = (s_I(\tau), s_Q(\tau))^T$  satisfies to the vector integral equation

$$\mathbf{s}(\tau) = (1/2) \int_0^{\tau_0} \hat{K}(|\tau - \tau'|) \mathbf{s}(\tau') d\tau' + \mathbf{s}^*(\tau) \quad (10)$$

with the core matrix (see [20] )

$$\hat{K}(\tau) = \begin{pmatrix} E_1(\tau) & b[E_1(\tau) - 3E_3(\tau)] \\ b[E_1(\tau) - 3E_3(\tau)] & 2b^2[5E_1(\tau) - 12E_3(\tau) + 9E_5(\tau)] \end{pmatrix} \quad (11)$$

and the primary source term

$$\mathbf{s}^*(\tau) = (1/2) \{E_3(\tau) - E_3(\tau_0 - \tau), b[E_3(\tau) - E_3(\tau_0 - \tau) - 3(E_5(\tau) - E_5(\tau_0 - \tau))]\}^T. \quad (12)$$

Here  $b = \sqrt{1/8}$ ,  $E_n(\tau) = \int_0^1 e^{-\tau/\mu} \mu^{n-2} d\mu$  is the  $n$ -th integral exponent.

For the intensity change  $\Delta I/I_0 \equiv (I - B)/B$  and for the polarization degree of radiation emerging through the boundary  $\tau = 0$  we obtain from eq. (9)

$$\begin{aligned} \Delta I/I_0 &= (v/c)a_\nu r(\mu, \tau_0) + O((v/c)^2), \\ Q/I &= -(v/c)a_\nu P(\mu, \tau_0) + O((v/c)^2), \end{aligned} \quad (13)$$

where the profiles of intensity change and polarization are

$$\begin{aligned} r(\mu, \tau_0) &= \mu \left(1 - e^{-\tau_0/\mu}\right) + \int_0^{\tau_0} e^{-\tau/\mu} \left[s_I(\tau) + (1/\sqrt{8})(1 - 3\mu^2)s_Q(\tau)\right] d\tau/\mu, \\ P(\mu, \tau_0) &= -(3/\sqrt{8})(1 - \mu^2) \int_0^{\tau_0} e^{-\tau/\mu} s_Q(\tau) d\tau/\mu. \end{aligned} \quad (14)$$

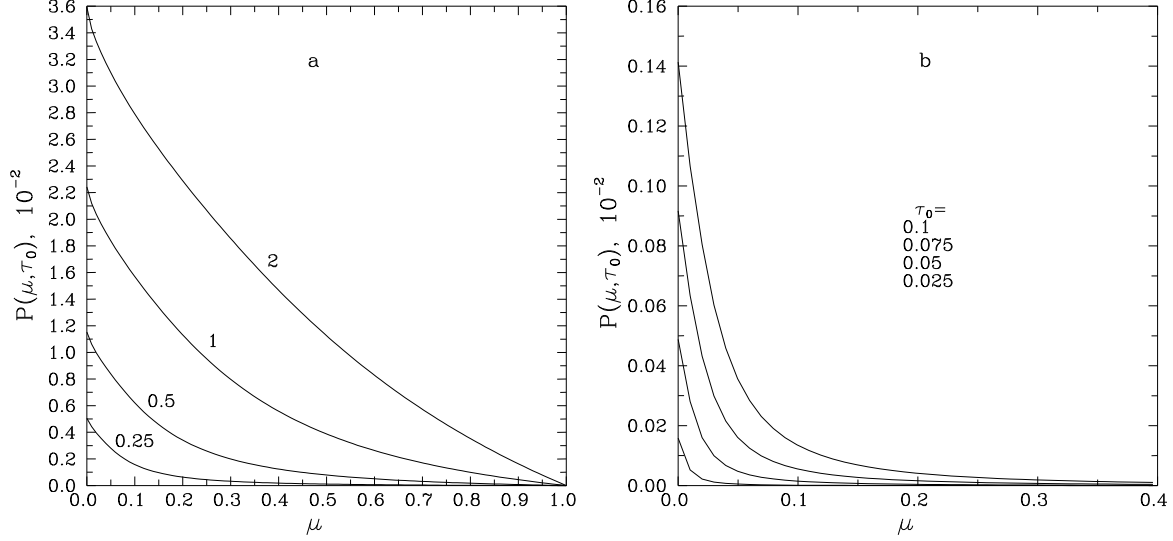


Figure 2: Profiles of polarization for Rayleigh scattering for different values of  $\tau_0$  marked near the curves (a) or listed in the same order as the curves follow, from up to down, (b).

For the maximum polarization degree which is reached at  $\mu = 0$  and for the corresponding intensity change we have from eq. (14)

$$\begin{aligned} P(0, \tau_0) &= -(3/\sqrt{8})s_Q(0), \\ r(0, \tau_0) &= s_I(0) + (1/\sqrt{8})s_Q(0). \end{aligned} \quad (15)$$

For the radiation emerging through the boundary  $\tau = \tau_0$  we obviously should change the sign of  $v$  in the formulae above i.e. to change the sign of polarization and intensity variation.

Integral equation (10) was solved numerically by discretization at some  $\tau$  grid and reducing to the system of linear algebraic equations for the values of the source function at the knots of the grid. These values are used then to calculate the profiles of the intensity change and polarization through eq. (14). The results are shown in Figs. 1 and 2.

As we can see in Fig. 2b there is a strong dependency of polarization degree on  $\mu$  for small  $\tau_0$ . For  $\tau_0 \ll 1$  we obtain the following expansions for  $s_I(\tau)$  and  $s_Q(\tau)$  with the accuracies up to the first and second order on the optical depth respectively:

$$\mathbf{s}(\tau) = \begin{pmatrix} s_I(\tau) \\ s_Q(\tau) \end{pmatrix} \sim \begin{pmatrix} -\tau + \tau_0/2 \\ (\tau_0/8\sqrt{2})[(\tau_0 - 2\tau)(C + 1/2) - \tau \ln \tau + (\tau_0 - \tau) \ln(\tau_0 - \tau)] \end{pmatrix}, \quad (16)$$

where  $C = 0.577216$  is the Euler constant. Substitution of these expansions into eqs. (14) and (15) gives us the analytical expressions of the intensity change and polarization profiles for  $\tau_0 \ll 1$ :

$$r(\mu, \tau_0) \sim \begin{cases} \tau_0/2, & \mu \ll \tau_0, \\ \tau_0, & \mu \gg \tau_0, \end{cases} \quad (17)$$

$$P(\mu, \tau_0) \sim \begin{cases} P(0, \tau_0) \sim -(3/32)\tau_0^2(\ln \tau_0 + C + 1/2), & \mu \ll \tau_0, \\ -(1/64)\tau_0^4(1 - \mu^2)\mu^{-2}(\ln \tau_0 + C + 2/3), & \mu \gg \tau_0. \end{cases} \quad (18)$$

Eq. (18) explains the strong dependency of polarization degree on  $\mu$ . It is confirmed by numerical calculations. For example, at  $\tau_0 = 0.01$  its error is less than 4% for  $\mu > 0.09$ , at  $\tau_0 = 0.025$  is less than 4% for  $\mu > 0.14$  and at  $\tau_0 = 0.1$  is less than 10% for  $\mu > 0.13$ . We can obtain even more precise approximation taking into account the terms of larger order with respect to  $\tau_0$ . Thus, for  $P(0, \tau_0)$  we have

$$P(0, \tau_0) \approx -(3/32)\tau_0^2[(1 + 1.25\tau_0) \ln \tau_0 + C + 1/2], \quad (19)$$

the error of which is less than 1% for  $\tau_0 < 0.1$ .

An approximate analytical estimate of the maximum polarization degree for a homogeneous sphere with a small optical radius  $\tau_0$  was obtained by Sunyaev and Zel'dovich [16]:  $(Q/I)_{\max} = \pm(v_t/c)a_\nu\tau_0^2/10$ , where  $v_t$  is the transversal velocity. However, the accuracy of this estimate is unknown because it was not compared with numerical calculations.

Obtained dependencies of CMB intensity and polarization on layer parameters allow us to model observational manifestations of these objects. In the protoobject directions we would registrate increase or decrease of CMB intensity depending on the sign of velocity  $v$ . Having measured the intensity change, we may estimate the  $(v/c)\tau_0$  value through the eqs. (13) and (17). Numerical analysis of polarization in couple with intensity variation data would permit to obtain the values of velocity and optical thickness of the layer separately.

### 3 Resonance scattering

Let us consider now the case of CMBR scattering in a spectral line, say, in a line of  $HeH^+$  with the laboratory wavelength  $149\mu$ . At  $z = 150$  this corresponds to the wavelength  $2.25$  cm.

We use the model of two-level atoms with the transition frequency  $\nu_{12}$ . Let  $x$  be the dimensionless frequency:  $x = (\nu - \nu_{12})/\Delta\nu_D$ , where  $\Delta\nu_D$  is the Doppler width of the line. Let  $\phi(x)$  be the absorption coefficient profile normalized as follows:  $\int_{-\infty}^{\infty} \phi(x)dx = 1$ .

Since we have axial symmetry again, the Stokes vector  $\mathbf{i}$  will have only two components ( $I$  and  $Q$ ). But now it will depend not only on coordinate and direction ( $\tau$  and  $\mu$ ) but on frequency  $x$ . The radiative transfer equation is written as (see [21] for example):

$$\begin{aligned} \mu \frac{\partial \mathbf{i}(\tau, \mu, x)}{\partial \tau} &= \phi(x) \mathbf{i}(\tau, \mu, x) - \frac{\lambda}{2} \int_{-1}^1 d\mu' \int_{-\infty}^{\infty} \hat{R}(\mu, x; \mu', x') \mathbf{i}(\tau, \mu', x') dx' - \mathbf{s}^*(\tau, \mu, x) \equiv \\ &\equiv \phi(x) \mathbf{i}(\tau, \mu, x) - \mathbf{s}(\tau, \mu, x). \end{aligned} \quad (20)$$

The matrix  $\hat{R}(\mu, x; \mu', x')$  describes the redistribution over frequencies, angles and polarization conditions at a single scattering,  $\lambda$  is the single scattering albedo,  $\mathbf{s}^*(\tau, \mu, x)$  is the primary source function vector. If there is no primary sources embedded in the layer it is defined by illumination from outside:

$$\mathbf{s}^*(\tau, \mu, x) = \frac{\lambda}{2} \int_{-\infty}^{\infty} dx' \int_0^1 \hat{R}(\mu, x; \mu', x') \left[ e^{-(\tau_0 - \tau)\phi(x')/\mu'} \mathbf{i}_2(\mu', x') + e^{-\tau\phi(x')/\mu'} \mathbf{i}_1(-\mu', x') \right] d\mu', \quad (21)$$

where  $\mathbf{i}_1(\mu, x) = \mathbf{i}_2(\mu, x) \sim B(\nu_{12}, T)[1 - (v/c)a_{\nu_{12}}\mu]\mathbf{e}_1$ ,  $a_{\nu_{12}} = x_{12}/(1 - e^{-x_{12}})$ ,  $x_{12} = h\nu_{12}/kT$ ,  $\mathbf{e}_1 = (1, 0)^T$ . As in the case of Rayleigh scattering we use below dimensionless Stokes vector and vector source function (measured in the units of  $B(\nu_{12}, T)$ ).

We use the assumption of complete frequency redistribution, according to which (see [21])  $\hat{R}(\mu, x; \mu', x') = \phi(x)\phi(x')\hat{P}(\mu, \mu') = \phi(x)\phi(x')\hat{A}(\mu)\hat{A}^T(\mu')$ , where  $\hat{A}(\mu)$  is defined by eq. (5). The value of depolarization parameter  $W$  in that equation is defined by the quantum numbers of the total angular momentum of the upper and the lower levels of transition (see [19] for example). Polarization becomes smaller as  $W$  decreases.  $W = 1$  corresponds to dipole scattering. In this case the phase matrix is the same as for the Rayleigh scattering.

The factorization of the redistribution matrix  $\hat{R}(\mu, x; \mu', x')$  leads to factorization of the source term in the righthandside of eq. (20):  $\mathbf{s}(\tau, \mu, x) = \phi(x)\hat{A}(\mu)\mathbf{s}(\tau)$ . Then we use the procedure described in [21] to reduce the problem to the solution of the linear integral equation of the type (10) for a vector source function  $\mathbf{s}(\tau)$  depending only on the optical depth. But now the elements of the core matrix  $\hat{K}(\tau)$  in eq. (10) are (see [21]):

$$\begin{aligned} K_{11}(\tau) &= \lambda \int_{-\infty}^{\infty} \phi^2(x) E_1(\phi(x)\tau) dx, \\ K_{12}(\tau) &= K_{21}(\tau) = b\lambda \int_{-\infty}^{\infty} \phi^2(x) [E_1(\phi(x)\tau) - 3E_3(\phi(x)\tau)] dx, \\ K_{22}(\tau) &= 2b^2\lambda \int_{-\infty}^{\infty} \phi^2(x) [5E_1(\phi(x)\tau) - 12E_3(\phi(x)\tau) + 9E_5(\phi(x)\tau)] dx. \end{aligned} \quad (22)$$

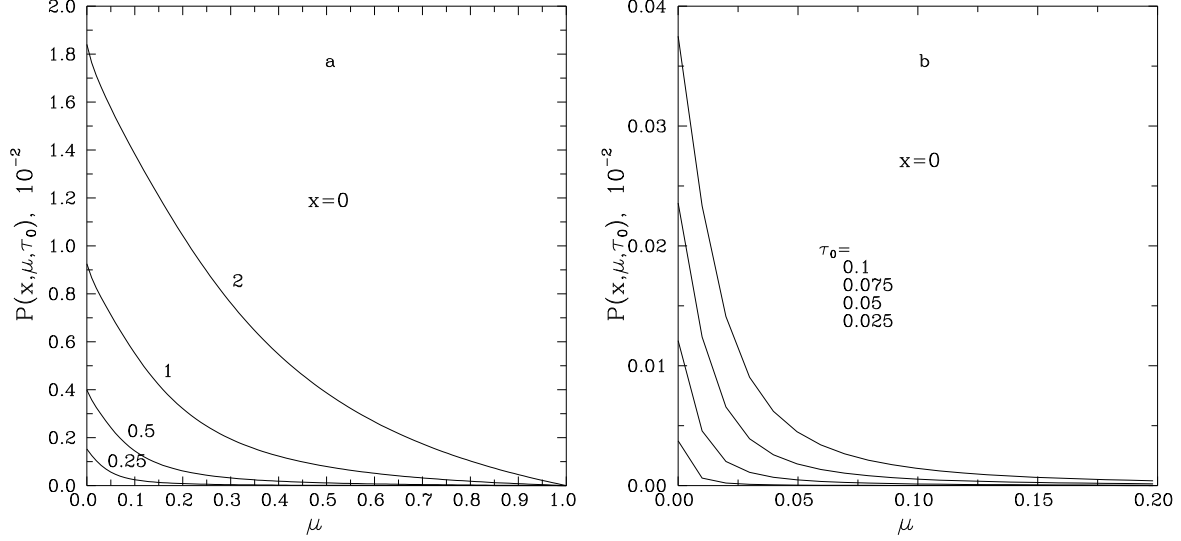


Figure 3: Angular profiles of polarization in a center of a spectral line for different values of  $\tau_0$  marked near the curves (a) or listed in the same order as the curves follow, from up to down, (b).

Finally we obtain the following expression for the Stokes vector of emerging radiation:

$$\mathbf{i}(0, \mu, x) = \mathbf{e}_1 + (v/c)a_{\nu_{12}}\mu \left(1 - e^{-\tau_0/\zeta}\right) \mathbf{e}_1 - (1 - \lambda)[1 + (v/c)a_{\nu_{12}}\mu] \hat{A}(\mu) \int_0^{\tau_0} e^{-\tau/\zeta} \mathbf{s}_0(\tau) d\tau / \zeta + \\ + (v/c)a_{\nu_{12}} \hat{A}(\mu) \int_0^{\tau_0} e^{-\tau/\zeta} \mathbf{s}(\tau) d\tau / \zeta, \quad \mu > 0, \quad (23)$$

where  $\zeta = \mu/\phi(x)$ ,  $\mathbf{s}_0(\tau)$  is the solution of type (10) equation with the free term  $\mathbf{s}^* = \mathbf{e}_1$ , and  $\mathbf{s}(\tau) = (s_I(\tau), s_Q(\tau))^T$  is the solution of the same equation but with the free term  $\mathbf{s}^* = (s_I^*, s_Q^*)^T$ :

$$s_I^* = \frac{\lambda}{2} \int_{-\infty}^{\infty} \phi(x) [E_3(\phi(x)\tau) - E_3(\phi(x)(\tau_0 - \tau))] dx, \quad (24)$$

$$s_Q^* = \frac{\lambda}{2} b \int_{-\infty}^{\infty} \phi(x) \{ [E_3(\phi(x)\tau) - E_3(\phi(x)(\tau_0 - \tau))] - 3 [E_5(\phi(x)\tau) - E_5(\phi(x)(\tau_0 - \tau))] \} dx. \quad (25)$$

Since for the most part of molecules the value of  $1 - \lambda$  is about  $10^{-9}$  and the value of  $v/c$  is about  $10^{-4}$ , we may neglect the term proportional to  $1 - \lambda$  in eq. (23). However, the account of this term does not bring any difficulties.

As in the case of Rayleigh scattering we introduce the intensity change and polarization profiles of the emerging radiation at  $\tau = 0$  in analogy to eq. (13) where now according to eq. (23)

$$r(x, \mu, \tau_0) = \mu \left[ 1 - e^{-\phi(x)\tau_0/\mu} \right] + \phi(x) \int_0^{\tau_0} e^{-\phi(x)\tau/\mu} \left[ s_I(\tau) + \sqrt{W/8} (1 - 3\mu^2) s_Q(\tau) \right] d\tau / \mu, \\ P(x, \mu, \tau_0) = -3\sqrt{W/8} (1 - \mu^2) \phi(x) \int_0^{\tau_0} e^{-\phi(x)\tau/\mu} s_Q(\tau) d\tau / \mu. \quad (26)$$

For the maximum polarization which is reached at  $\mu = 0$  and for the corresponding intensity change we have from above equations

$$P(x, 0, \tau_0) = -3\sqrt{\frac{W}{8}} s_Q(0), \\ r(x, 0, \tau_0) = s_I(0) + \sqrt{\frac{W}{8}} s_Q(0). \quad (27)$$

Note that these quantities do not depend on  $x$ .

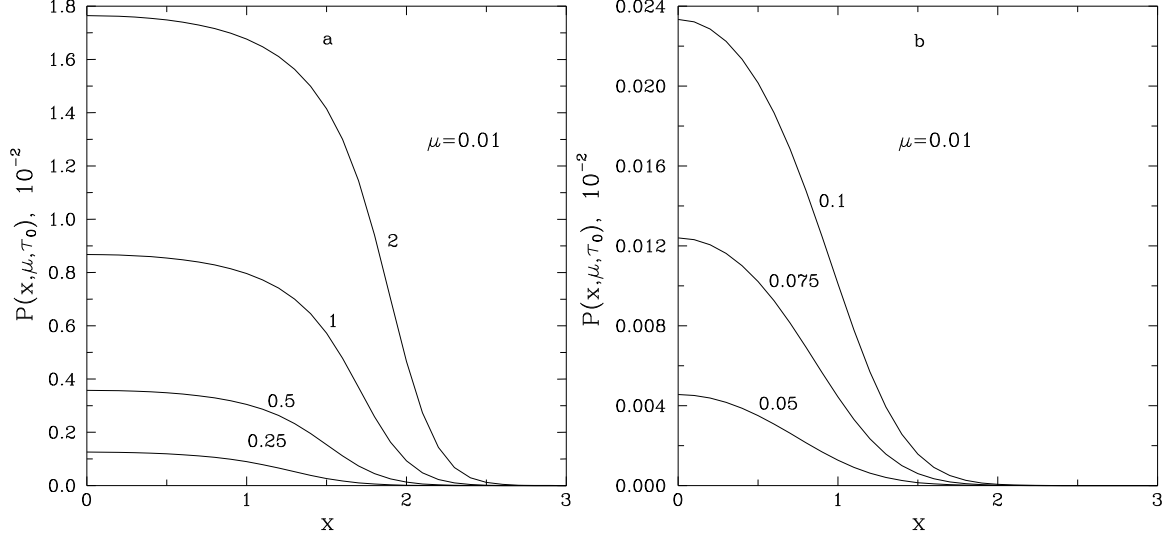


Figure 4: Frequency profiles of polarization in a spectral line for different values of  $\tau_0$  marked near the curves.

The integral equation (10) with the core matrix and free term, given by eqs. (22) and (24-25) respectively, was solved numerically as in the case of Rayleigh scattering. We have used the Doppler profile  $\phi(x) = \pi^{-1/2}e^{-x^2}$  and brought  $W = 1$ ,  $\lambda = 1$ . These values of parameters  $W$  and  $\lambda$  evidently maximize the degree of polarization. Fig. 3 shows the dependency of polarization  $P$  on the angular variable  $\mu$  in the center of the line ( $x = 0$ ) for different values of the optical thickness  $\tau_0$ . Comparing Figs. 2 and 3 we see that the resonance polarization is lower a bit than the Thomson one, that is quite expectable. Fig. 4 shows the dependency of  $P$  on dimensionless frequency  $x$  inside the line for different values of  $\tau_0$ . We can see that with increasing of  $\tau_0$  the line becomes wider, which is natural since the number of scatterings rises. The same is true for intensity. The dependency of polarization on  $\mu$  for  $\tau_0 = 0.5$  and different frequencies is shown in the Fig. 5a. We can see that this dependency is very sharp in the wings of the line, which is explained by small optical thickness there. Finally, the dependence of  $P$  on  $x$  for different values of  $\mu$  is shown in the Fig. 5b. With the decrease of  $\mu$  the line becomes wider since the optical path along the line of sight increases.

For  $\tau_0 \ll 1$  we can obtain the following expansions for the components of the vector source function:

$$\begin{aligned} s_I(\tau) &\sim \frac{\lambda}{2} \frac{1}{\sqrt{2\pi}} (\tau_0 - 2\tau), \\ s_Q(\tau) &\sim \frac{\lambda}{4\pi} \sqrt{\frac{W}{8}} \left\{ \frac{1}{\sqrt{3}} \left[ \tau_0(\tau_0 - 2\tau)(C - 1/6) - \tau^2 \ln \frac{\tau}{\sqrt{\pi}} + (\tau_0 - \tau)^2 \ln \frac{\tau_0 - \tau}{\sqrt{\pi}} \right] + \right. \\ &\quad \left. + \frac{\lambda}{2} \left[ \tau(\tau_0 - \tau) \ln \frac{\tau_0 - \tau}{\tau} + \frac{\tau_0}{2}(\tau_0 - 2\tau) \right] \right\}. \end{aligned} \quad (28)$$

Substituting these expansions into eqs. (26) and (27) we obtain the following expressions for the CMB intensity change and polarization profiles (for the observer reference frame):

$$r(x, \mu, \tau_0) \sim \begin{cases} (\lambda/2)\tau_0/\sqrt{2\pi}, & \mu \ll \tau_0\phi(x), \\ \phi(x)\tau_0, & \mu \gg \tau_0\phi(x), \end{cases} \quad (29)$$

$$P(x, \mu, \tau_0) \sim \begin{cases} -\frac{3}{32} \frac{\lambda W}{\pi} \tau_0^2 \left[ \frac{1}{\sqrt{3}} \left( C - \frac{1}{6} + \ln \frac{\tau_0}{\sqrt{\pi}} \right) + \frac{\lambda}{4} \right], & \mu \ll \tau_0\phi(x), \\ -\frac{1}{64} \frac{\lambda W}{\pi} \phi^2(x) \frac{1 - \mu^2}{\mu^2} \tau_0^4 \left[ \frac{1}{\sqrt{3}} \left( C - \frac{1}{4} + \ln \frac{\tau_0}{\sqrt{\pi}} \right) + \frac{3}{8} \lambda \right], & \mu \gg \tau_0\phi(x). \end{cases} \quad (30)$$

At low values of  $\tau_0$  the last formula is in a good agreement with the results of numerical calculations. For example, the polarization dependency on  $\tau_0$  is quite sharp ( $\sim \tau_0^4$ ) for  $\mu \gg \tau_0\phi(x)$ , but is more slow ( $\sim \tau_0^2$ ) for



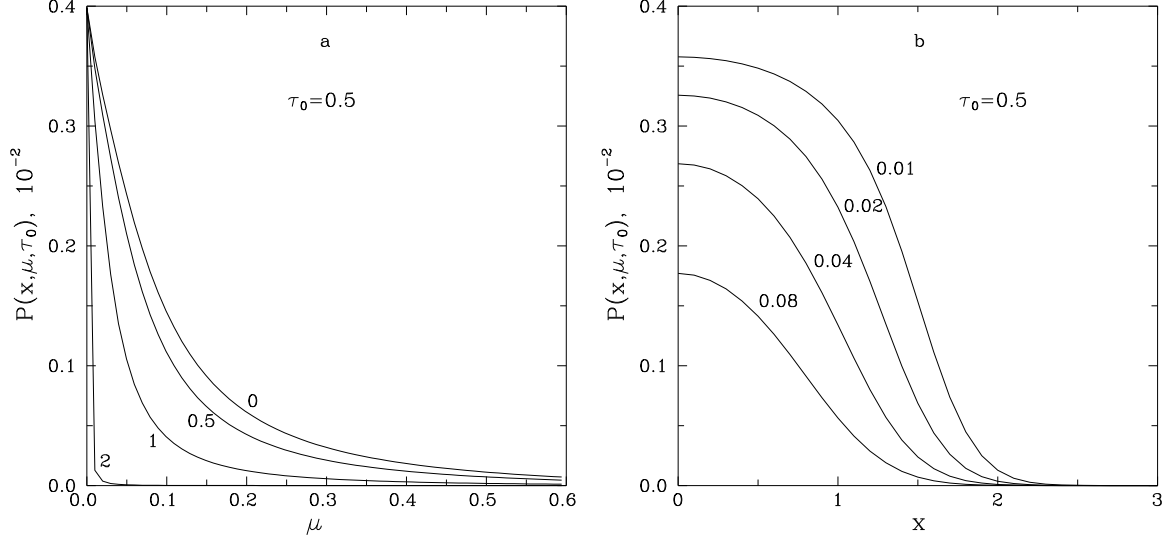


Figure 5: Profiles of polarization in a spectral line: a) for different frequencies  $x$  (marked near the curves), b) for different values of  $\mu$  (marked near the curves).

$\mu \ll \tau_0 \phi(x)$ . For approximate estimation of polarization the accuracy of eq. (30) is quite enough. For example, at  $\tau_0 = 0.01$  and  $\mu > 0.1$  its error is less than 3.5%.

## 4 Conclusion

In this work we investigate the possible observational display of Thomson scattering on free electrons and of resonance scattering in a spectral line of cosmic microwave background radiation in the flat moving layers from “dark ages” epoch ( $10 < z < 1000$ ). The formulae for appearing anisotropy and polarization of CMB are obtained and numerical calculations are made. We show that for characteristic parameters according to recent models of substance evolution at that period the values of intensity fluctuations and polarization of cosmic microwave background may be in the following ranges:  $\Delta I/I_0 = 10^{-4} \div 10^{-6}$ ,  $Q/I = 10^{-6} \div 10^{-7}$ . The effects are observable and their discover would be a sufficient forward step in investigations of substance evolution in the pre-galactic epoch.

We do not consider a transfer of the calculated intensity and polarization changes through a homogeneous universe from  $z \approx 150$  to  $z = 0$ . The possible distortions caused by such a transfer are defined by an optical thickness of the universe due to Thomson scattering. According to the recent measurements in the BOOMERANG and MAXIMA experiments (see [22], [23]) the Thomson optical thickness of the universe between  $z = 0$  and  $z = 1100$  is evaluated to be less than 0.1. As we concerned by an interval between  $z = 0$  and  $z \approx 150$  the distortions of the calculated fluctuations will not exceed probably a few percents which is undoubtedly less than an uncertainty of the protoobject models.

**Acknowledgements.** We are grateful to Yu. Parijskij, V. Ivanov, D. Nagirner and A. Starobinsky for the interest and useful discussions. This research is supported in part by Grant # 00-15-96607 under the program “Leading Scientific Schools” and by Grant # 02-02-16535 from the Russian Foundation for Basic Research.

## References

- [1] V.K. Dubrovich, *Astronomy Letters*, **3**, 243, 1977.
- [2] A.G. Doroshkevich, Ya.B. Zeldovich, R.A. Sunyaev, “Formation and evolution of Galaxies and Stars”, M., Nauka, 1976 (in Russian).
- [3] Ya.B. Zeldovich, I.D. Novikov, “Structure and Evolution of the Universe”, M., Nauka, 1975 (in Russian).
- [4] S.F. Shandarin, A.G. Doroshkevich, Ya.B. Zeldovich, *Uspehi Fizicheskikh Nauk*, **139**, 83, 1983 (in Russian).
- [5] P.J.E. Peebles, “The large-scale structure of the Universe”, Princeton University Press, Princeton, N. J., 1980.
- [6] A. Knebe, V. Muller, *Astron. Astrophys.*, **341**, 1, 1999.
- [7] N.A. Bahcall, *Comments in Astrophysics*, **11**, 283, 1987.
- [8] V.K. Dubrovich, *Astron. Astrophys.*, **324**, 27, 1997.
- [9] V.K. Dubrovich, *Astronomical and Astrophysical Transactions*, **5**, 57, 1994.
- [10] V. Dubrovich, B. Partridge, *Astronomical and Astrophysical Transactions*, **19**, 233, 2000.
- [11] A. Doroshkevich, V. Dubrovich, astro-ph/0108213, 2001.
- [12] A. Jenkins et al., *Astrophys. J.*, **499**, 20, 1998.
- [13] P. Shapiro, astro-ph/0104315, 2001.
- [14] V.K. Dubrovich, *Astronomy Letters*, **27**, 207, 2001.
- [15] S. Lepp, M. Shull, *Astrophys. J.*, **280**, 465, 1984.
- [16] R.A. Sunyaev, Ya.B. Zeldovich, *Mon. Not. R. Astron. Soc.*, **190**, 413, 1980.
- [17] Ya.B. Zeldovich, R.A. Sunyaev, *Astronomy Letters*, **6**, 285, 1980.
- [18] R.A. Sunyaev, Ya.B. Zeldovich, in R. Sunyaev, ed., Soviet Scientific Reviews Sect. E: *Astrophysics and Space Physics Rev.*, vol. 1. Harwood Academic Publishers, New York, p. 1, 1981.
- [19] S. Chandrasekhar, “Radiative Transfer”, Oxford, 1950.
- [20] V.V. Ivanov, *Astron. Astrophys.*, **303**, 609, 1995.
- [21] V.V. Ivanov, S.I. Grachev, V.M. Loskutov, *Astron. Astrophys.*, **318**, 315, 1997.
- [22] P. De Bernardis et al., *Nature*, **404**, 905, 2000.
- [23] A. Jaffe et al., astro-ph/0007333, 2000.